BMC Chemistry

RESEARCH ARTICLE

Open Access

Ultrastructural changes in the fat body of desert locust, *Schistocerca gregaria* (Orthoptera: Acrididae) treated with zinc chromium oxide nanostructures via chemical co-precipitation approach

Fatma M. Hashem[1], Elsayed Elgazzar[2] and Wageha A. Mostafa[1*]

Abstract

The present work aims to investigate the ultrastructural changes in the fat body of fifth instar nymphs *Schistocerca gregaria* (Orthoptera: Acrididae) treated with zinc chromium oxide (ZnCrO). The nanoparticles (NPs) were prepared by co-precipitation route and characterized using X-ray diffraction (XRD), energy dispersive X-ray spectroscopy (EDX), scanning electron microscopy (SEM), and transmission electron microscopy (TEM). The ZnCrO NPs exhibited polycrystalline hexagonal structure, composed of spherical–hexagonal shapes with an average size ~ 25 nm. Besides, the UV–Vis spectrophotometer (Jasco-V-570) was utilized for optical measurements. The energy gap (E_g) was estimated from the transmittance (T%) and reflectance (R%) spectra through the range of 3.307–3.840 eV. In biological sections, *S. gregaria* 5th instar nymphs, TEM images demonstrated that the fat body was strongly impacted with the concentration 2 mg NPs result in great agglomeration of chromatin in the nucleus as well as haemoglobin cells (HGCs) pierced with malformed trachea (Tr) at 5th and 7th days post treatment. The obtained results indicated a positive action of the prepared nanomaterial on *Schistocerca gregaria* fat body organelles.

Keywords Ultrastructure, Fat body, *Schistocerca gregaria*, ZnCrO NPs, Nanospheres, Energy gap

*Correspondence:
Wageha A. Mostafa
wageha.elhalaby@yahoo.com; Wamostafa@zu.edu.eg
Full list of author information is available at the end of the article

Graphical Abstract

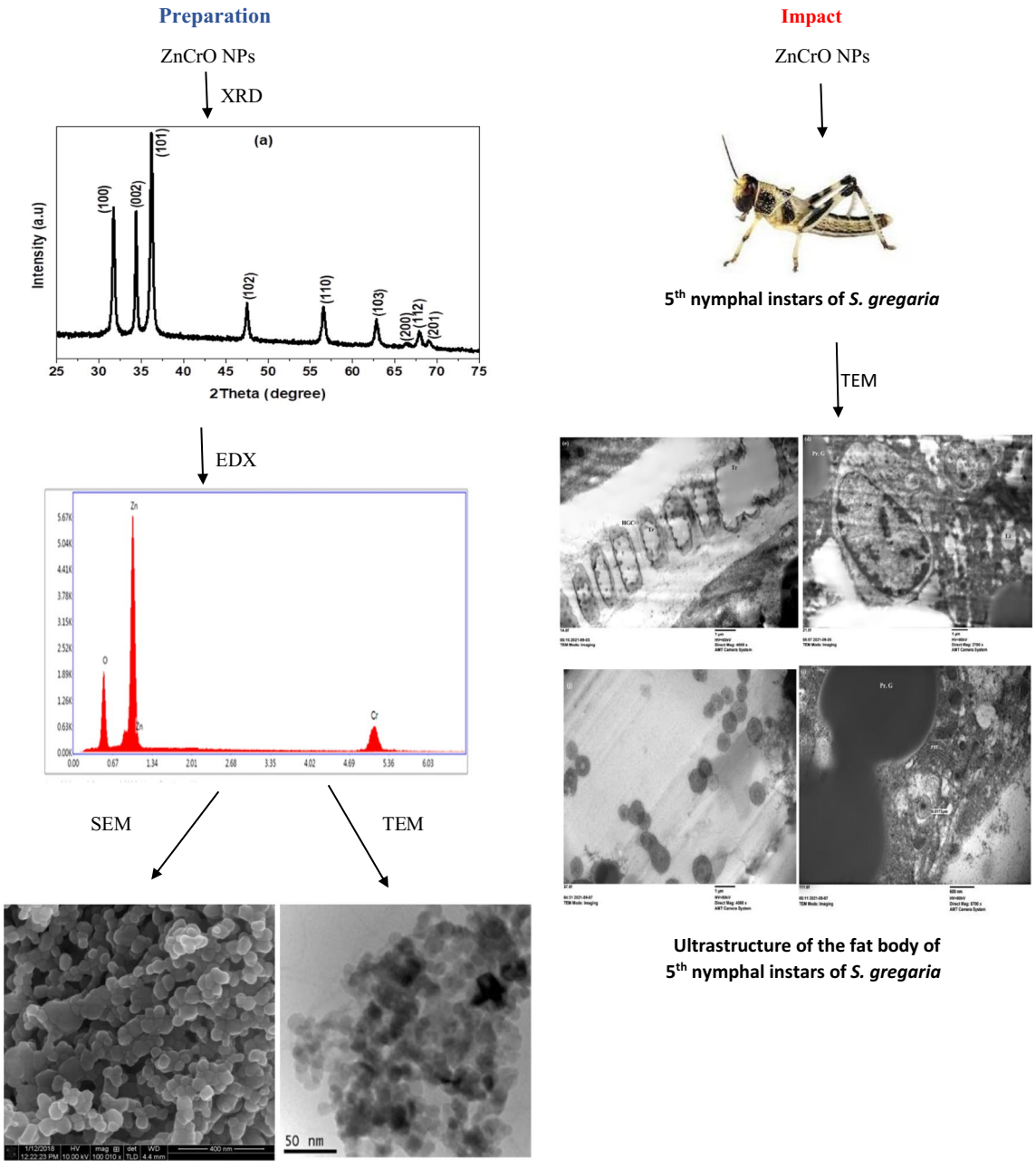

Introduction

Nanotechnology is considered one of the modern and attractive fields owing to its advantages and wide range applications extend from chemical engineering and communication systems to biotechnological activities. Currently, nanomaterials are utilized in agriculture and expected to revolutionize the field of pest management in the near future. The importance of this technology has emerged in offering novel ways for designing active ingredients and crop protection [1–3]. Several studies have used the nanoparticles (NPs) to replace traditional chemical pesticides against weeds, plants pathogens,

and insect pests dependence of their safety toward the environment and human beings [4]. Unlike conventional hydrophobic pesticides, nanocides may be water-soluble (hydrophilic) which enhances bioactivity and coverage uniformity. Because they can be applied in small volumes and taken up quickly by cells, the use of nanocides can slow the development of resistance in target pests [5–7]. Recently, metal oxide based nanoparticles, such as magnesium oxide (MgO), tin oxide (SnO_2), titanium dioxide (TiO_2), silver oxide (Ag_2O), and zinc oxide (ZnO) have been used in biosensors, catalysis, biomedical imaging, optoelectronic devices, and medicine industry. Specifically, ZnO nanostructures of low toxicity level, small crystallite size, high chemical reactivity, and good chemical stability can be used in biological fields without hazardous beneficial organisms [8]. Keerthana et al. [9] have reported the distinctive aspects of ZnO NPs in the agricultural field as biogenesis for protecting yield food crops and improving the growth of *Abelmoschus esculentus* in a safe and nontoxic regime. However, promoting of structural and physical characteristics of ZnO by doping with appropriate transition metal like Cu, Mn, Fe, Co, Ag, Ru, Pd, etc. have important role in many of technological areas. Among the integrated possibilities, inducing chromium (Cr) ions into ZnO framework revealed great advantages owing to the small ionic radius of chromium ions (0.062 nm) compared with zinc ions (0.074 nm) as well as their similar electronegativity values [10]. These aspects enable Cr^{3+} to be easily incorporated inside the host ZnO lattice structure producing new energy levels inside the band gap, increasing of free charge and transport density. Debnath et al. [11] have improved the physical properties of pure ZnO by chromium ions synthesized by chemical approach. It is worth noting that integrating Cr3+ inside ZnO leads to increase active sites and surface to volume area [11]. The desert locust, *Schistocerca gregaria* [12–14] is a species of locust, a periodically swarming, short-horned grasshopper in the family Acrididae. They are found primarily in the deserts and dry areas of northern and eastern Africa, Arabia, and southwest Asia. The desert locust shows periodic changes in its body form and can change in response to environmental conditions, over several generations, from a solitary, shorter-winged, highly fecund, non-migratory form to a gregarious, long-winged, and migratory phase in which they may travel long distances into new areas. In some years, they may thus form locust plagues, invading new areas, where they may consume all vegetation including crops, and at other times, they may live unnoticed in small numbers. The desert locust's migratory nature and capacity for rapid population growth present

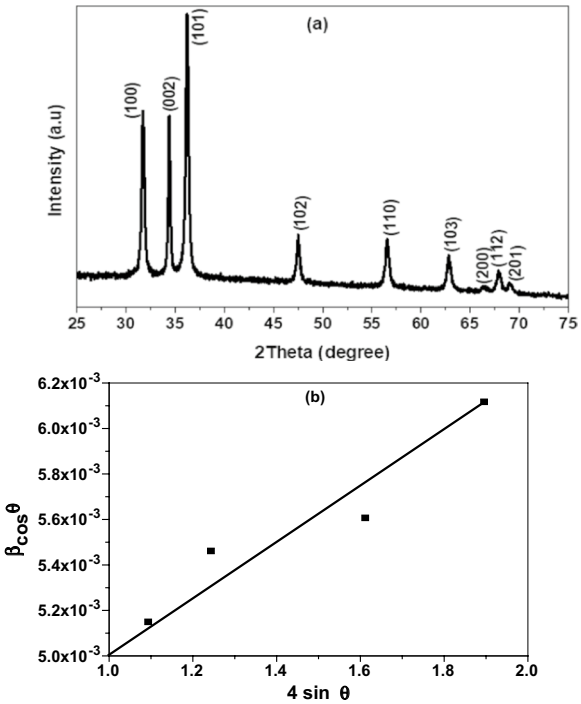

Fig. 1 **a** XRD pattern of ZnCrO and **b** W–H method of Cr doped ZnO nanopowder annealed at 450 °C

major challenges for control, particularly in remote semi-arid areas, which characterize much of their range [15]. The fat body of *Schistocerca gregaria* is an important target of toxic metals and is involved in multiple homeostatic functions regulating nutrient synthesis and storage or providing several metabolic pathways [16, 17]. The peripheral fat body of *Schistocerca gregaria* (Orthoptera: Acrididae) occupies the peripheral portion, which presents an anatomical relation showing a delicate granular, long striped shape, irregular distribution reaching the anterior portion of the prothorax [18]. Fat bodies have important roles in detoxification, endocrinology, reproduction and nutrition, so damage to this organ may indicate relevant sublethal effects that may comprise insect development and behavior [19, 20]. Nanopesticides that penetrate the organisms of insects leading to mortality have attracted much attention throughout the current decade [20, 21]. Nanometal oxides can be developed by using various chemical and physical techniques such as hydrothermal microwave irradiation, combustion synthesis, magnetron sputtering, sol–gel, and electrochemical methods [22, 23]. The current study was undertaken to synthesize and characterize ZnCrO NPs by chemical co-precipitation reaction and to study its impact on the fat body of *S. gregaria* fifth instar nymphs.

Experimental section

Materials and methods

Preparation and characterization of zinc chromium oxide nanopowder

$Zn_{1-x}Cr_xO$ nanopowder (x = 10 wt%) was prepared by a cost-effective chemical co-precipitation. In this chemical reaction, 12.15 g zinc acetate dihydrate $[Zn(CH_3COO)_2{\cdot}2H_2O]$ was dissolved in 55 ml deionized water and 2.65 g chromium acetate dihydrate $[Cr_2(OOCCH_3)_4{\cdot}2H_2O]$ in 20 ml using magnetic stirrer. Chromium acetate was slowly added to zinc acetate solution with continuous stirring for 2 h at the room temperature. Then, 4.15 g sodium hydroxide (NaOH) was dissolved in 55 ml deionized water and gradually added dropwise to aqueous zinc/chromium acetate solution with stirring at constant speed (900 rpm/min) for 5 h. A homogeneous white gray precipitate powder was formed at pH ~ 9. After that, the obtained powder was washed, dried at 80 °C for 12 h and eventually calcined at 450 °C for 3 h.

Characterization of the nanomaterial

The prepared ZnCrO was characterized by XRD (Rigaku Smart Lab.) at wavelength λ = 1.54 Å (Cu Kα radiation) with 2θ angle changed from 25° to 75°. Energy dispersive X-ray analysis (EDX) attached with scanning electron micrograph (SEM; Helios Nanolab. 400) were examined to identify the element composition and surface morphology. Before the SEM technique, the sample was bombarded with evaporated conductive iridium (Ir) atoms via a spin coater sputter coater (Model, EMS 150T ES). To identify the mean size and particle distribution, transmission electron microscopy (TEM; Hitachi-H-7500) was employed at 100 kV. The UV–Vis spectrophotometer JASCO (V-570) was utilized for measuring transmittance and reflectance spectra and determination of the type of energy gap transition. The thin films were prepared by dissolving 5 mg of ZnCrO NPs into 15 ml ethanol/dimethylformamide (DMF). The solution was deposited drop by drop on the glass substrates using spin coating technique. Thereafter, the fabricated thin films were left for drying in a furnace at 200 °C for 1 h.

Insect rearing

Individuals of the desert locust, *S. gregaria* were obtained from the Plant Protection Research Institute, Zagazig, Sharkia Governorate, Egypt. Adults were reared in the laboratory under crowded conditions at 30 ± 2 °C, 70–80% R. H. and a photoperiod of 8 D: 16 L for several generations. Adults were placed in wooden-framed cages measuring 40 × 40 × 60 cm as described by [24, 25].

Table 1 Crystallographic parameters of $Zn_{1-x}Cr_xO$ nanostructure

Metal oxide NPs	D (nm)		ε × 10^{-4}	δ × 10^{-4} (nm^{-2})	Sa × 10^5 (cm^2/g)
	Scherer	W–H			
$Zn_{1-x}Cr_xO$	33.30	36.00	11.00	8.00	3.00

Treatment

The experimental design was arranged with four groups of treatments and three replicates, and each experiment consisted of ten 5th instar nymphs of *S. gregaria*. The first group was sprayed with 0.150 mg of zinc chromium oxide NPs, the second group was sprayed with 1 mg of zinc chromium oxide, the third group was sprayed with 2 mg of zinc chromium oxide and the fourth group was a control.

Electron microscope studies

Nymphal instars from the 4 tested groups were prepared for electron microscopy by anesthetizing them with CO_2 and then killing them by twisting the head to break the "neck" membrane and collecting the peripheral fat body of the thorax at intervals of 3, 5 and 7 days post treatment which was immobilized by chilling for a few minutes on ice.

They were dissected in ice- cold Ringer's solution (86 ml M NaCl, 5.4 ml M KCl, 3 ml $MCaCl_2 \times 2H_2O$ containing a small amount of phenylthiourea) and transferred to a fixative consisting of 2.5% glutaraldehyde (Sigma) in 0.1 M cacodylate buffer (pH 7.2) for approximately 10 min, dissected free and put into fresh fixative for 1–2 h. after washing in 0.1 M cacodylate buffer, the specimens were postfixed in 1% OsO4 in the same buffer for 1 h, washed, dehydrated in an ethanol series, and embedded in Araldite epoxy resin.

Semithin sections for light microscopy and ultrathin sections for electron microscopy (EM) were cut on a Leica EM KMR2 ultramicrotome. The Semithin sections were stained with toluidine blue, meanwhile Ultrathin sections (80 nm) were stained with 4% uranyl acetate and 0.4% lead citrate in distilled water and examined with a JEOL 1200 EX II transmission electron microscope at the central laboratory, Faculty of Science, Zagazig University.

Results and discussion

Crystallographic, elemental composition, and microstructure analysis of $Zn_{1-x}Cr_xO$ NPs

Figure 1a illustrated the XRD pattern of Cr-doped ZnO annealed at 450 °C for 3 h. As shown, the nanopowder of polycrystalline structure nature with a wurtzite hexagonal phase and matching with the standard XRD data (JCPDS card no: 36-1451, space group P63mc) [26, 27].

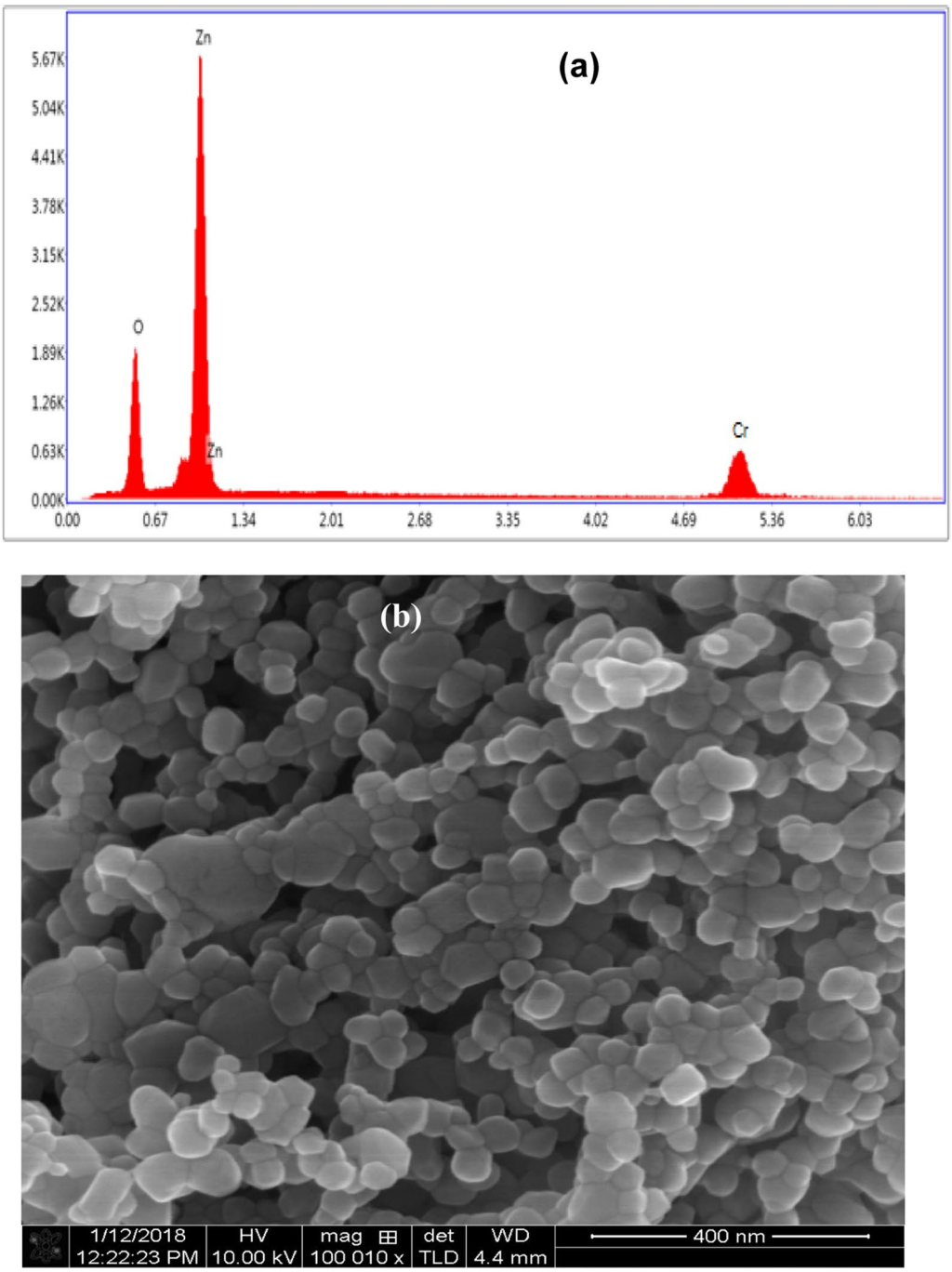

Fig. 2 **a** EDX spectrum, **b** SEM micrographs, and **c** TEM image of the ZnCrO nanoparticles annealed at 450 °C

The sharp peaks distinguished by high intensity revealing the high crystallinity degree. No extra peaks attributed to hydroxyl (–OH) groups, chromium oxide (Cr_2O_3) or chromium metal ions Cr^{3+} are observed in the pattern, which emphasize the purity of the nanostructure [27, 28]. Additionally, the close electronegativity values of Zn (1.65) and Cr (1.65) as well as the small ionic radius of chromium ions (0.062 nm) led to Cr^{3+} easily incorporated into the ZnO lattice [29, 30]. The crystallite size (D) of the nanoparticles was evaluated from the Scherer formula and confirmed by the Williamson–Hall (W–H) method using the following equations [31, 32]:

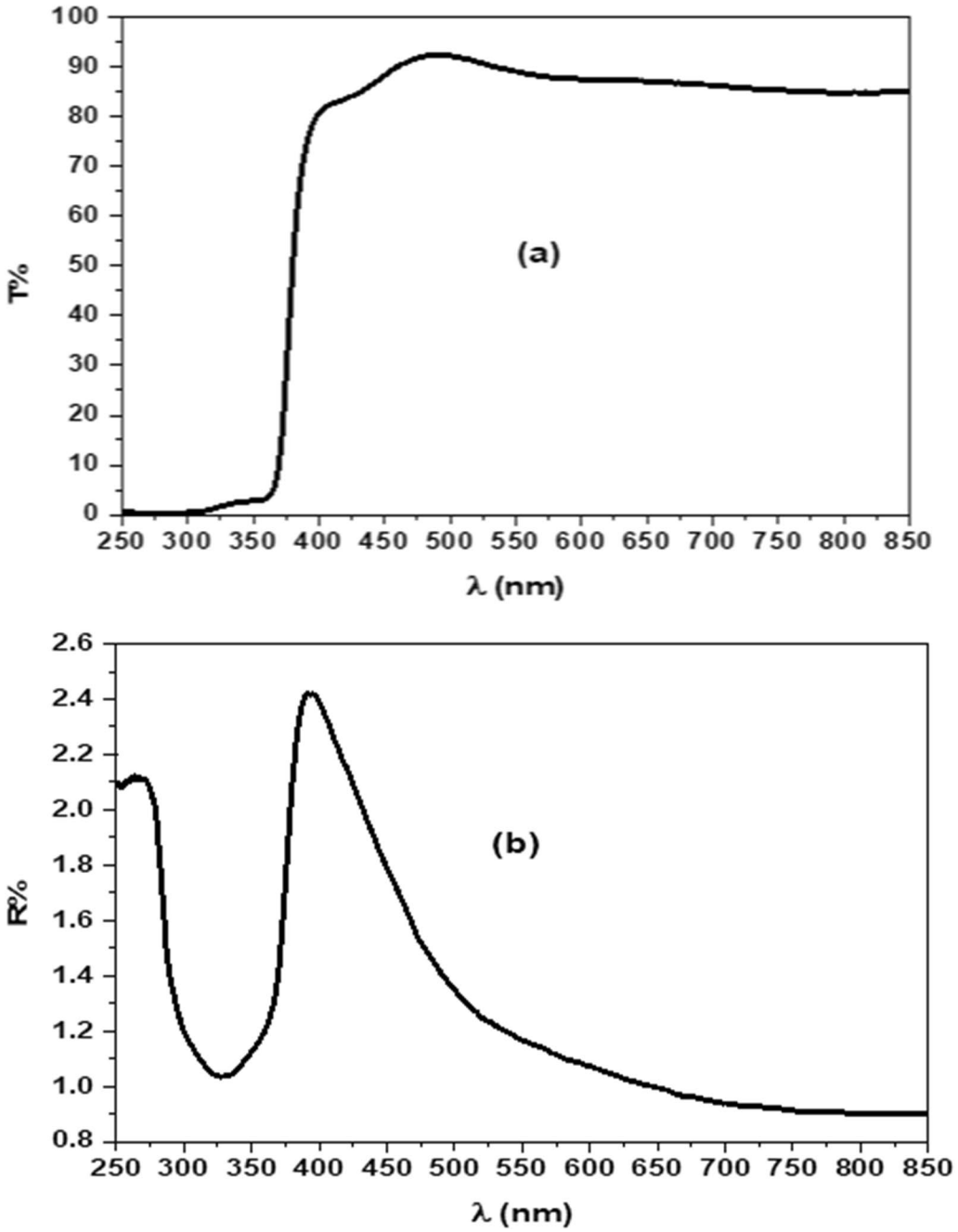

Fig. 3 **a** Transmittance spectrum (T%) and **b** reflectance spectrum R%) of $Zn_{1-x}Cr_xO$ thin film

$$D = \frac{K\lambda}{\beta \cos\theta}, \tag{1}$$

$$\beta \cos\theta = \frac{k\lambda}{D} + 4\varepsilon \sin\theta, \tag{2}$$

where λ is the X-ray wavelength equals 1.540 Å for Cu Kα, k is the shape factor of constant value equals 0.94, β is the FWHM representing instrumental broadening, θ is Bragg's scattering angle, and ε is the lattice strain. The Scherer equation was applied on the strongest peak of the preferred, Miller indices (hkl 101) which used to determine the planes and lattice dimensions. Moreover, the Williamson–Hall (W–H) equation was defined from $\beta \cos\theta$ to $4 \sin\theta$ plot, illustrated in Fig. 1b. The results obtained from W–H method are more accurate

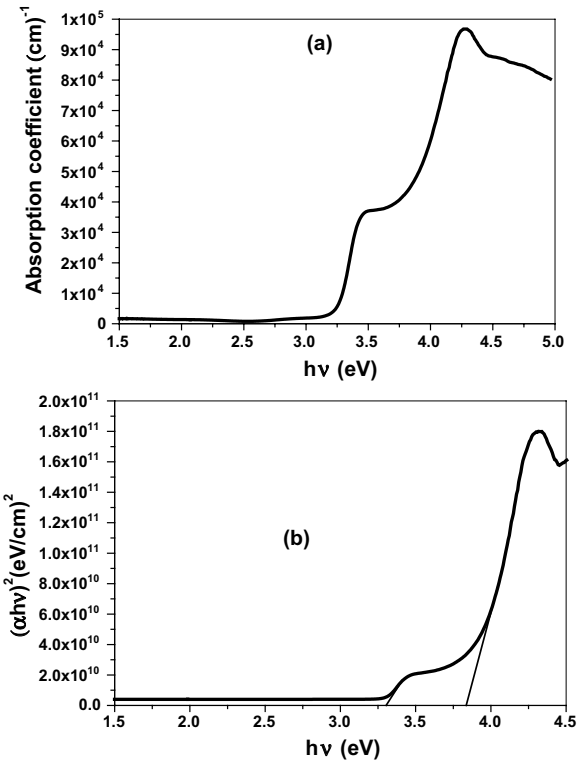

Fig. 4 **a** Optical absorption coefficient and **b** (αhν) 2 versus hν plot for $Zn_{1-x}Cr_xO$ thin film

compared to Scherer equation in which both crystallite size and the influence of strain are involved through the XRD planes [31, 33]. As demonstrated in Fig. 1b, the strain (ε) was determined from the slope and the crystallite size (D) from the intercept $\left(\frac{k\lambda}{D}\right)$ by knowing the values of k and λ. The dislocation density (δ) was evaluated by the relation [32, 33]:

$$\delta = \frac{1}{D^2}, \tag{3}$$

and the specific surface area (S_a) was given by [31]:

$$S_a = \frac{6}{D \times \rho}. \tag{4}$$

Here ρ is the density equal to 5.58 g/cm^3 for zinc chromium oxide. The XRD parameters were calculated and summarized in Table 1. As tabulated, ZnCrO NPs exhibited small size approximately equal to 36 nm and a relatively large specific surface area attributed to generate more charge carriers by chromium ions replacement. Furthermore, the chemical composition and purity of the synthesized nanomaterial were investigated using EDX spectroscopy, Fig. 2a. As observed, the spectrum composed of the main elements Zn, Cr, and O only with atomic percent (at.%) 58.67, 8.86, and 32.47 respectively, which is consistent with the starting composition. The presence of chromium (Cr) in the spectrum clearly supports the successful integration chemical reaction and formation of zinc chromium oxide compound with pure phase [34]. For further microstructure analysis, SEM micrograph was done to visualize the surface topology and shape of the nanoparticles. As depicted in Fig. 2b, the particles are distributed in nanosphere/hexagonal like structures, where some of them agglomerated together [30, 34]. Besides, the mean size of the nanospheres was estimated from the TEM image to be around 25 nm (Fig. 2c) [35, 36].

Optical properties of Cr-doped ZnO thin film

Figure 3a describes the optical transmittance (T%) of ZnCrO thin film through the wavelength range of 250–850 nm. The film exhibited high transmittance above 85% within the visible region of a sharp absorption edge detected at 380 nm associated with electron interband transitions from the valence band to the conduction band [37, 38]. Further, the optical reflectance (R%) displayed valleys and peaks inside the UV region and near the visible spectrum related to the optical-electron interactions, (Fig. 3b). The absorption coefficient (α) of was calculated by the equation described as [39, 40]:

$$\alpha = \frac{1}{d} \ln \left[\frac{(1 - R^2)}{2T} + \sqrt{\frac{(1 - R)}{4T^2} + R^2} \right]. \tag{5}$$

The absorption coefficient (α) versus photon energy (hν) is presented in Fig. 4a. As shown, the film of a weak absorption peak in the UV spectrum while has a strong peak inside the visible region suggesting the strong light absorption and an increase of free charge carriers [40, 41]. The energy gap (E_g) is very important parameter in the semiconductor materials and transparent

(See figure on next page.)

Fig. 5 Electron microscope section of fat body cells of untreated 5th instar nymphs of *S. gregaria*. **a**–**c** View of fat body cells showing the general structure of the tissue on 3rd day, protein granules (Pr. G) (×2700), glycogen vacuole (Gl V), haemoglobin cells pierced with the trachea (Tr), lipid droplets (×4000X), nucleus (Nu) with chromatin (ch), lipid droplets (Li) (×2700). **d** Shows protein granules (Pr. G) (×2000) on the 5th day. **e** Protein granules (Pr. G), haemoglobin cells (HGC) pierced by the trachea (×2000) on the 7th day

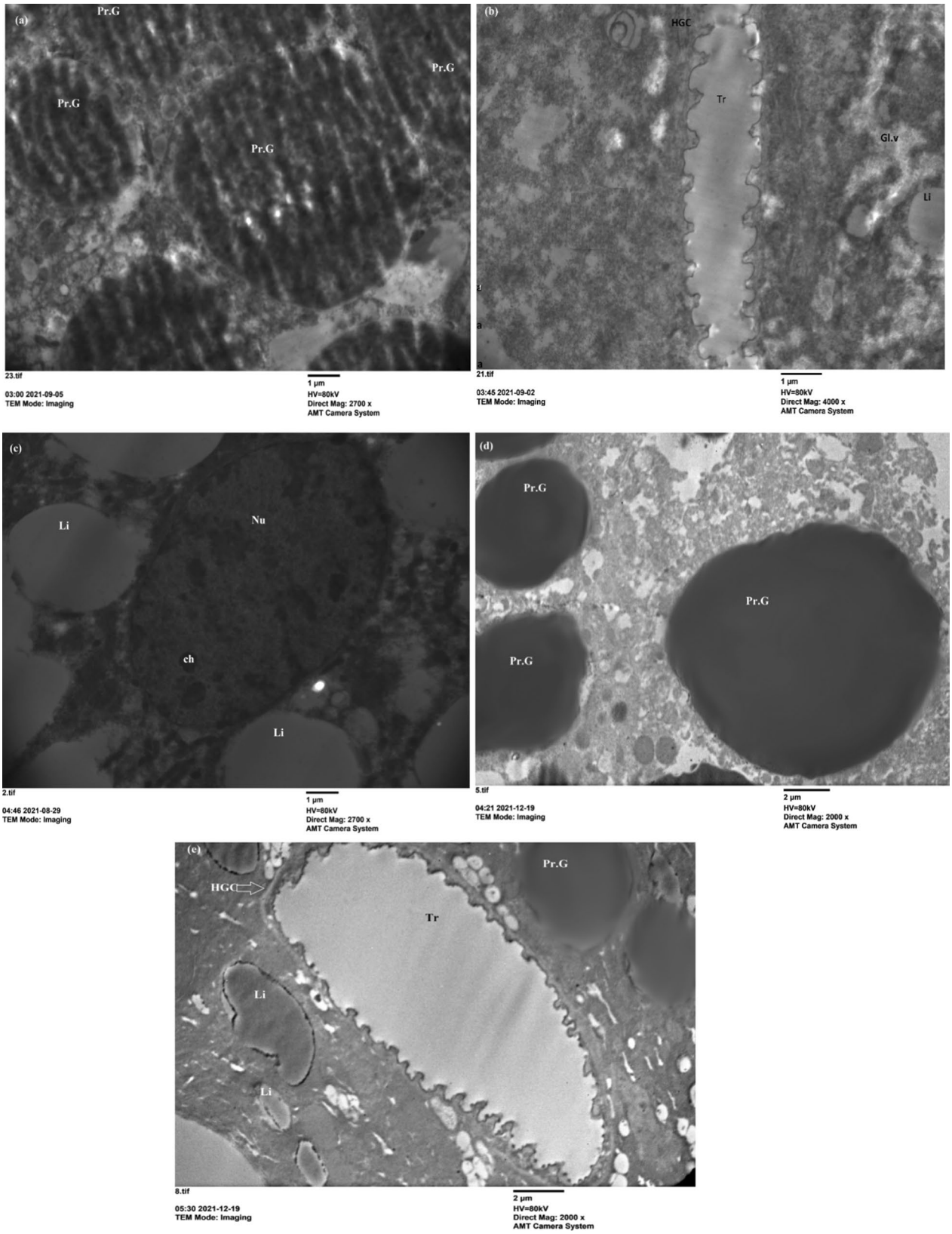

Fig. 5 (See legend on previous page.)

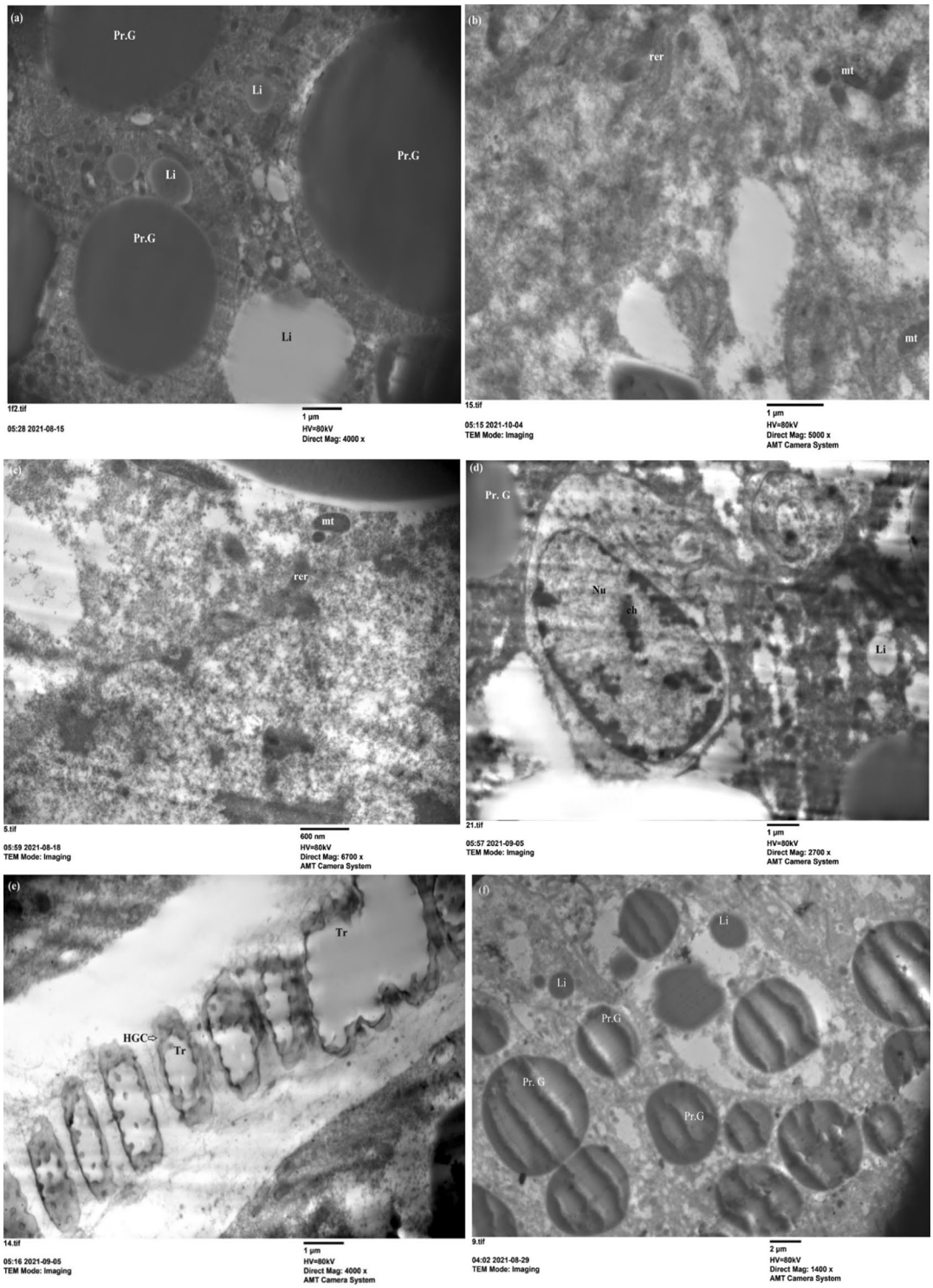

Fig. 6 Electron microscope section of fat body cells of treated 5th instar nymphs of *S. gregaria* sprayed with 2 mg of zinc chromium oxide. **a**, **b** View of fat body cells showing protein granules (Pr. G), lipid droplets (Li) (×4000); rough endoplasmic reticulum (rer), mitochondria (mt) (×5000) on the 3rd day post treatment. **c**–**e** Show rough endoplasmic reticulum (rer), mitochondria (mt) (×6700); nucleus (Nu) with chromatin clumps (ch), lipid droplets (Li) (×2700); haemoglobin cells pierced with the trachea (Tr) (×4000) on the 5th day post treatment. **f** Protein granules (Pr. G), lipid droplets (Li) (×1400) on the 7th day post treatment. **g**–**i** Show Protein granules (Pr. G) and crystals of nanoparticles (4000, 2700, ×6700) on the 7th day post treatment. **j** Crystals of ZnCrO around the tissues of fat body (×4000) on the 7th day post treatment

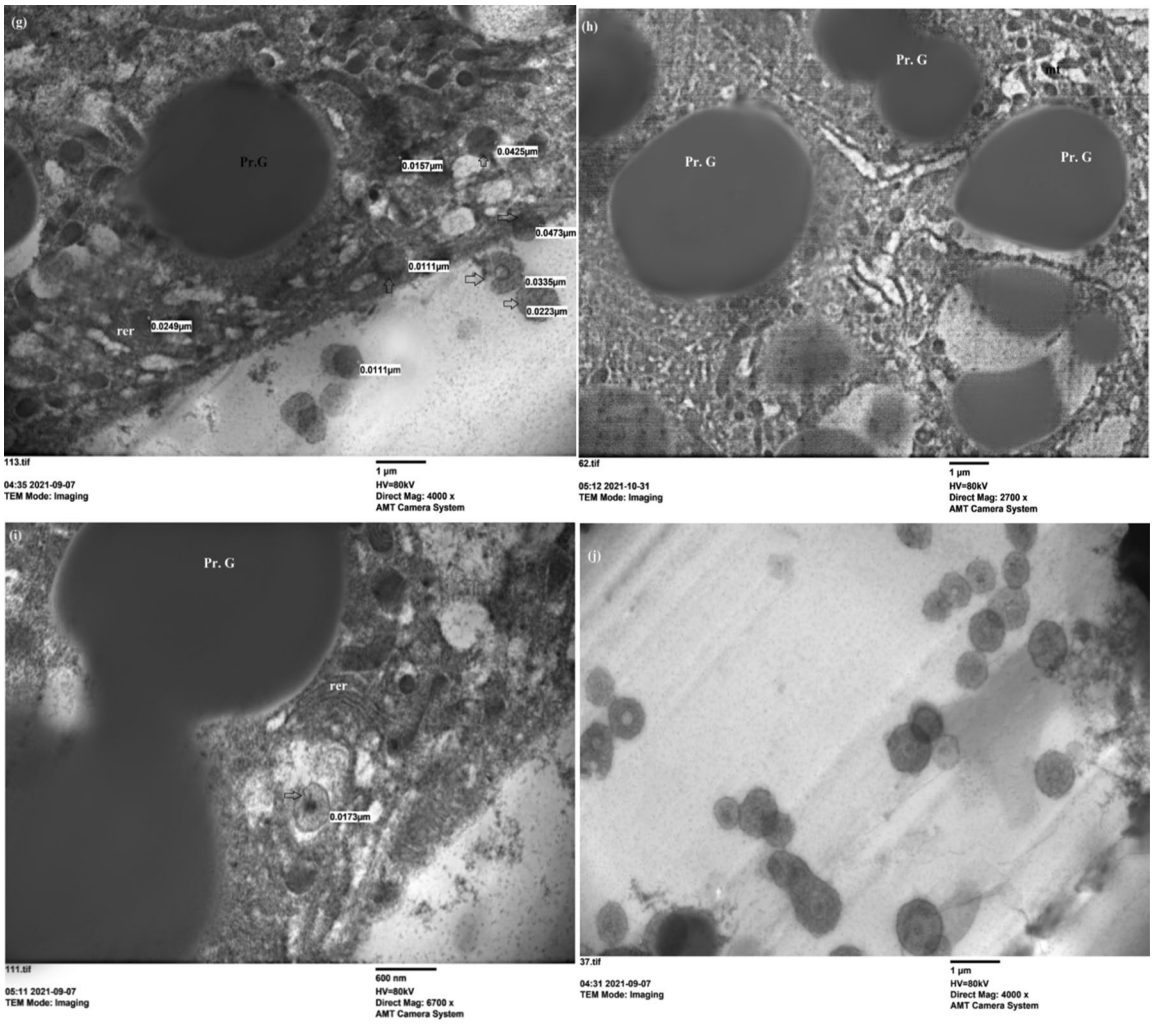

Fig. 6 continued

nanometal oxides was determined from $(\alpha h\nu)^2$ against $(h\nu)$ plot (Fig. 4b) according to Tauc's relation expressed as [40, 41]:

$$\alpha = \frac{A}{h\nu}\left(h\nu - E_g\right)^n. \quad (6)$$

A is independent constant and $n = 1/2$ for direct band gap. By extrapolating the linear portion to $(\alpha h\nu)^2 = 0$, the energy gap of the fabricated thin film was calculated within the visible spectrum in the range 3.307–3.840 eV [42, 43]. The observed high electron transitions and the reduction in the band gap by doping chromium ions results in the surface defects and releasing free Zn^{2+} and Cr^{3+} [11]. In addition to generating reactive oxygen species (ROS) which strongly impact on the disturbance of cellular equilibrium and cell causing locust death.

(See figure on next page.)

Fig. 7 Electron microscope section of fat body cells of treated 5th instar nymphs of *S. gregaria* sprayed with 1 mg of zinc chromium oxide. **a**–**c** Show rough endoplasmic reticulum (rer), nucleus (Nu) with chromatin clumps (ch) (×4000); protein granules (Pr. G) and nucleus (Nu) with chromatin clumps (ch) (×1400); lipid droplets (Li) (×2000) on the 3rd day post treatment. **d**, **e** Protein granules (Pr. G), nucleus (Nu) with chromatin clumps (ch), haemoglobin cells (HGC) pierced with the trachea (Tr) (×2700); haemoglobin cells (HGC) pierced with trachea (Tr) (×2000) on the 5th day post treatment. **f** Haemoglobin cells (HGC) pierced with the trachea (Tr) (×2700) on the 7th day post treatment

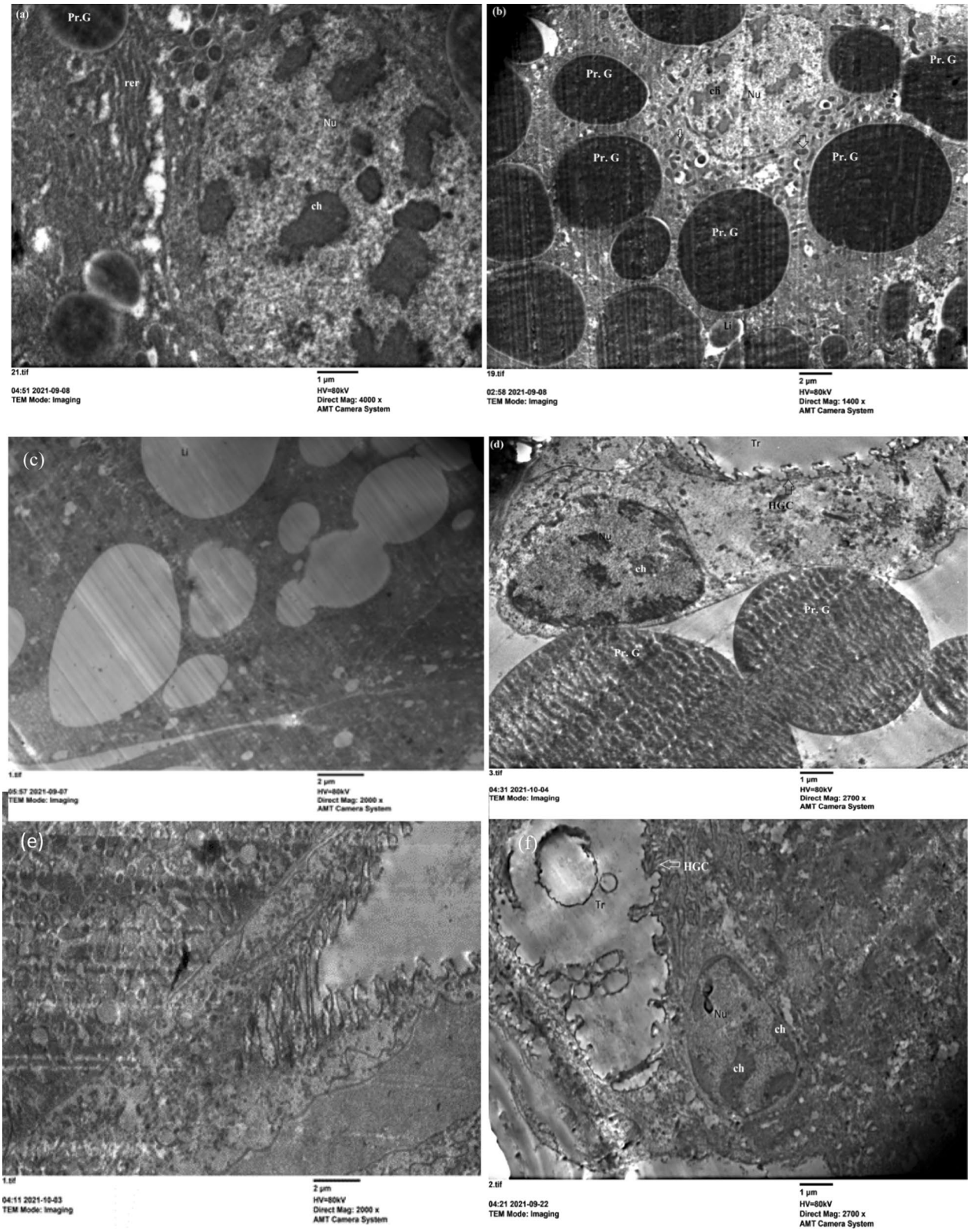

Fig. 7 (See legend on previous page.)

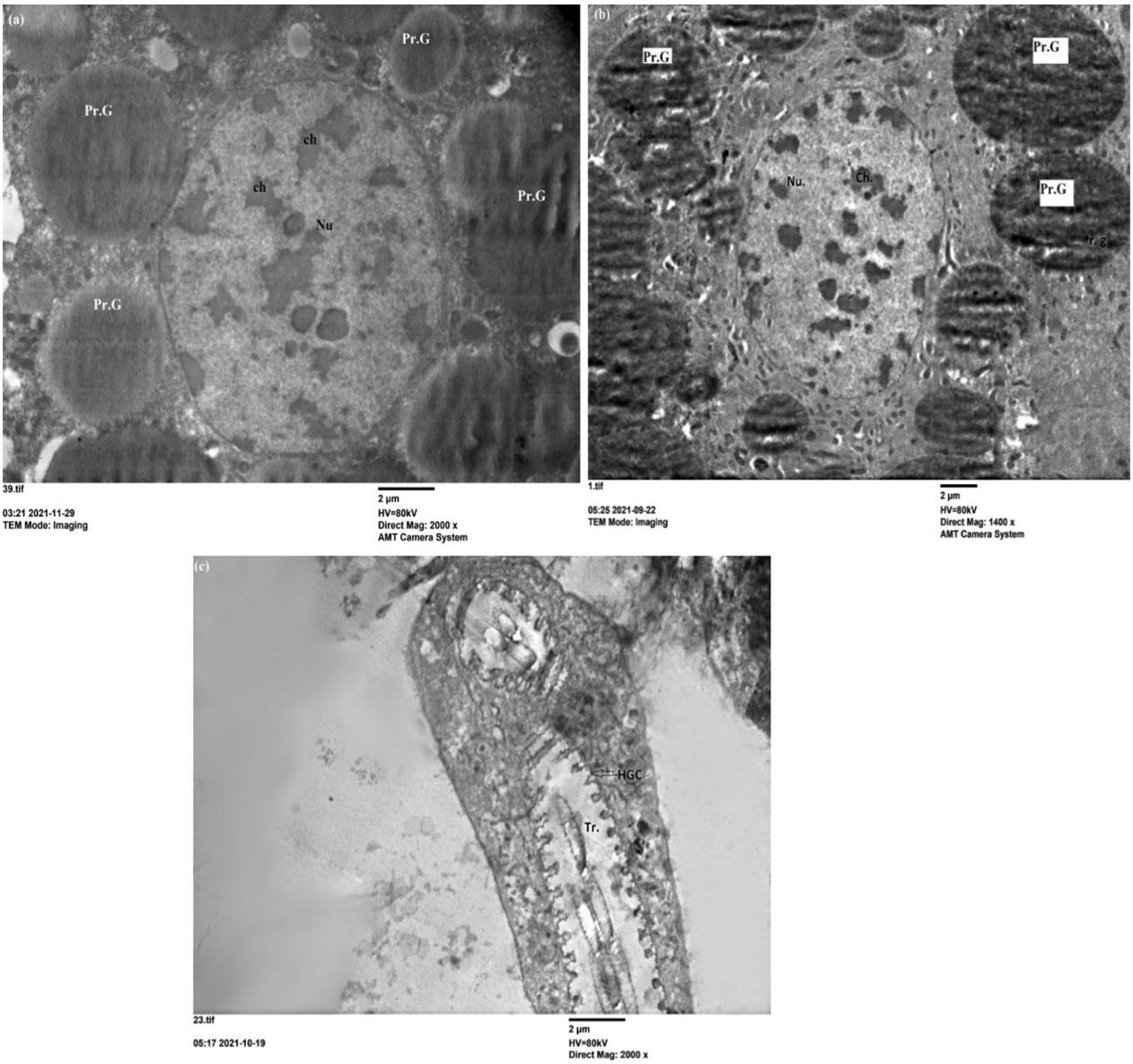

Fig. 8 Electron microscope section of fat body cells of treated 5th instar nymphs of *S. gregaria* sprayed with 0.150 mg of on zinc chromium oxide. **a** Shows protein granules (Pr. G), nucleus (Nu) with chromatin clumps (ch) (×2000) on the 3rd day post treatment. **b** Protein granules (Pr. G), nucleus (Nu) with chromatin clumps (ch) (×1400) on the 5th day post treatment. **c** Haemoglobin cells (HGC) pierced with the trachea (Tr) (×2000) on the 7th day post treatment

Ultrastructure of the fat body of 5th instar nymphs of S. gregaria

The fat body has vital roles in the life of insects. It is involved in multiple metabolic functions. One of these functions is to store and release energy in response to the energy demands of the insect [44]. Transmission electron microscopy of the untreated 5th instar nymphs showed that the peripheral fat body cells contained protein granules (PrG) as crystalline storage granules (Fig. 5a, d). The mitochondria (mt) were oval, and the endoplasmic reticulum had the appearance of regular strings and bears ribosomes forming a rough endoplasmic reticulum (rer). The nucleus (Nu) was spherical and possessed chromatin clumps (Ch), which were sporadically scattered throughout the nucleus (Fig. 5c). Haemoglobin cells (HGCs) were pierced by trachea (Tr) and lipid droplets (Li) (Fig. 5b, e). Insect adipocytes store a large amount of lipid reserves as cytoplasmic lipid droplets. Lipid metabolism is necessary for growth and reproduction and provides the energy needed during extended nonfeeding periods [44–47]. The

previous literatures described the ultrastructure of the fat body as the lipids are deposited as small drops or in large vacuoles that may occupy most of the cytoplasm. The proteins form electron dense granules of variable sizes and shapes, in some cases appearing crystallized [47–52].

On the other hand, the treatment nymphs with 2 mg of ZnCrO NPs declared no effect on the fat body organelles at 3rd day of post treatment (Fig. 6a, b). But, at 5th day post treatment mitochondria was swollen and dilation of cristerana of rough endoplasmic reticulum were observed (Fig. 6c). The malformed nucleus has peripheral chromatin and haemoglobin cells (HGCs) pierced by destroyed trachea which affected the respiration process (Fig. 6d, e). After 7 days of spraying 2 mg of ZnCrO, numerous cytolysosomes that digest cytoplasmic organelles were illustrated and were indicative of cytoplasmic deterioration and leads to cell death [53] and protein granules were shrinked and effected on protein metabolism (Fig. 6f). Crystals of nanoparticles showed around protein granules (Fig. 6g–j). The mean average size of ZnCrO observed between the protein granules of the fat body of 5th instar nymphs was 26 nm. This agreed with the size of the particles used.

The effect of nanoparticles decreased when sprayed with 1 mg of ZnCrO compared to the high concentration. The protein granules, lipid droplets and nucleus appeared in normal shape on the 3rd day post treatment with nanoparticles (Fig. 7a–c). Although at 5th and 7th days post treatment abnormal nucleus with crowded chromatin (Fig. 7d) and malformed trachea (Fig. 7e, f) were detected. However, the lowest concentration (0.150 mg) NPs showed normal protein granules, nuclei, and trachea (Fig. 8a–c). This study demonstrated that the nanoparticles caused structural damage in the fat body cells of immature stages and could alter the development of locusts. These changes cause the malfunction of fat body cells, particularly at a high concentration, leading to nymphal death. Meng et al. [54] reported that *Bombyx mori* (Lepidoptera: Bombycidae) showed low resistance against Ag NPs to oxidative stress, affected cell apoptosis, and induced cell necrosis by regulating related protein metabolism and metabolic pathways. Ag NPs can also reduce the ability of silkworms to withstand oxidative stress and interfere with programmed cell death.

Furthermore, the fat body cell malformations in this work is agreed with those described in the fat body cells of different insects exposed to azadiractin, neem oil, plant-derived, and insecticides such as swollen mitochondria in the cristolysis process, dilated cisternae of the rough endoplasmic reticulum, the fusion of lipid droplets, and dilation of the perinucleus [55–61]. Moreover, although the fat body was not directly exposed to ZnCrO nanoparticles by injection, it is a good target in ecotoxicological studies.

Conclusions

Cr doped ZnO (10 wt%) nanopowder was successfully synthesized with cost-effective chemical co-precipitation technique. The XRD pattern indicated that the nanomaterial of polycrystalline structure in pure phase in which chromium ions incorporated into the host ZnO framework. The EDX spectrum confirmed the presence of Cr^{3+} inside ZnO lattice structure and production of ZnCrO compound. The crystallographic parameters $(D, \varepsilon, \delta, \rho)$ were calculated showing that the nanoparticles of small grain size ~ 36 nm. The surface topological aspects of ZnCrO revealed that the NPs of spherical–hexagonal shapes with large surface to volume area. The optical properties displayed the prepared thin film of high transparency in the visible region and wide energy gap. The fat body is a good target organ in ecotoxicological studies by providing the details of injuries and cellular response. However, it was not directly exposed to zinc chromium oxide NPs by intake or spraying.

Abbreviations

NPs	Nanoparticles
XRD	X-ray diffraction
EDX	Energy dispersive X-ray spectroscopy
SEM	Scanning electron microscopy
TEM	Transmission electron microscopy
HGCs	Haemoglobin cells
Pr. G	Protein granules
mt	Mitochondria
Li	Lipid droplets
GlV	Glycogen vacuole
Tr	Trachea
Nu	Nucleus
rer	Rough endoplasmic reticulum
Ch	Chromatin clumps

Author contributions

EE raising the idea, nanomaterials synthesis and physical characterization, and writing the original draft. WAM supervised the biological tests. FMH performed the biological tests and wrote the manuscript. EE revised the manuscript and supervised the research. FMH and WAM reviewed the manuscript. All authors read and approved the final manuscript.

Funding

Open access funding is provided by The Science, Technology & Innovation Funding Authority (STDF) in cooperation with The Egyptian Knowledge Bank (EKB). This work was supported by funds from Zagazig University, Egypt.

Availability of data and materials

The datasets used and/or analyzed during the current study available from the corresponding author on reasonable request.

Declarations

Ethics approval and consent to participate

Not applicable.

Consent for publication

Not applicable.

Competing interests

The authors declare that they have no competing interests.

Author details
[1]Entomology Section, Zoology Department, Faculty of Science, Zagazig University, Zagazig 44519, Egypt. [2]Department of Physics, Faculty of Science, Suez Canal University, Ismailia 41522, Egypt.

Received: 15 June 2022 Accepted: 2 February 2023
Published: 20 February 2023

References

1. Aftab M, Butt MZ, Ali D, Bashir F, Aftab HZ. Impact of copper doping in NiO thin films on their structure, morphology, and antibacterial activity against *Escherichia coli*. Ceram Int. 2020;46:5037–49. https://doi.org/10.1016/j.ceramint.2019.10.247.
2. Barkhordari A, Hekmatimoghaddam S, Jebali A, Khalili MA, Talebi A, Noorani M. Effect of zinc oxide nanoparticles on viability of human spermatozoa. Iran J Reprod Med. 2013;11:767–71.
3. Wiwanitkit V, Sereemaspun A, Rojanathanes R. Effect of gold nanoparticles on spermatozoa: the first world report. Fertil Steril. 2009;91:7–8. https://doi.org/10.1016/j.fertnstert.2007.08.021.
4. Yasur J, Rani P. Environmental effects of nano silver: impact on castor seed germination, seedling growth and plant physiology. Environ Sci Pollut Res. 2013;20:8636–48. https://doi.org/10.1007/s11356-013-1798-3.
5. Benelli G. Research in mosquito control: current challenges for a brighter future. Parasitol Res. 2015;114:2801–5. https://doi.org/10.1007/s00436-015-4586-9.
6. Elfeky AS, Salem SS, Elzaref AS, Owda'ME, Eladawy HA, Saeed MA, Awad AM, AbouZeid RE, Fouda A. Multifunctional cellulose nanocrystal/metal oxide hybrid, photodegradation antibacterial and larvicidal activities. Carbohydr Polym. 2020;230: 115711. https://doi.org/10.1016/j.carbpol.2019.11571.
7. Prasad AR, Basheer SM, Gupta IR, Elyas KK, Joseph A. Investigation on bovine serum albumin (BSA) binding efficiency and antibacterial activity of ZnO nanoparticles. Mater Chem Phys. 2020;24: 122115. https://doi.org/10.1016/j.matchemphys.2019.122115.
8. Halo M, Bułka K, Antos PA, Gren' A, Slanina T, Ondruška L, Tokárová K, Massányi M, Formicki G, Halo M, Massányi P. The effect of ZnO nanoparticles on rabbit spermatozoa motility and viability parameters in vitro. Saudi J Biol Sci. 2021;28:7450–4. https://doi.org/10.1016/j.sjbs.2021.08.045.
9. Keerthana P, Vijayakumar S, Vidhya E, Punitha VN, Nilavukkarasi M, Praseetha PK. Biogenesis of ZnO nanoparticles for revolutionizing agriculture: a step towards anti-infection and growth promotion in plants. Ind Crops Prod. 2021;170: 113762. https://doi.org/10.1016/j.indcrop.2021.113762.
10. Okeke IS, Agwu KK, Ubachukwu AA, Ezema FI. Influence of transition metal doping on physiochemical and antibacterial properties of ZnO–nanoparticles: a review. Appl Surf Sci Adv. 2022;8: 100227.
11. Debnath T, Chakraborty T, Bandyopadhyay A, Sharma S, Mahapatra AS, Das S, Sutradhar S. Modulation of structural, morphological and electrical charge transport property of Cr-doped ZnO nanomaterials prepared by chemical process. Mater Sci Eng B. 2022;280: 115688.
12. Species *Schistocerca gregaria* (Forskål, 1775): Orthoptera species file. https://Orthoptera.speciesfile.org. Accessed 16 Feb 2020.
13. *Schistocerca gregaria* (Desert locust) (*Gryllus gregarius*). www.uniprot.org. Accessed 16 Feb 2020.
14. Forsskål, Peter; Niebuhr, Carsten; pre-1801 imprint collection (Library of Congress) DLC (1775). Descriptiones animalium, avium, amphibiorum, piscium, insectorum, vermium. Ghent University. Hauniæ, ex officina Mölleri.
15. Economic and policy issues in Desert Locust management (S. Joffe, 1998). www.fao.org. Accessed 16 Feb 2020.
16. Kafel A, Bednarska K, Augustyniak M, Witas I, Szulińska E. Activity of glutathione transferase in *Spodoptera exigua* larvae exposed to cadmium and zinc in two subsequent generations. Environ Int. 2003;28:683–6. https://doi.org/10.1016/S0160-4120(02)00111-3.
17. Xia Q, Sun H, Hu X, Shy Y, Gu D, Zhang G. Apoptosis of *Spodoptera litura* larval haemocytes induced by heavy metal zinc. Chin Sci Bull. 2005;50:2856–60. https://doi.org/10.1007/BF02899656.
18. Adamski Z, Banaszkiewicz M, Ziemnicki K. Ultrastructural alterations induced by fenitrothion on fat body cells and midgut cells of *Tenebrio molitor* L. (Insecta, Coleoptera) larvae. J Biol Res. 2005;3:15–22.
19. Adamski Z, Radtke K, Kopiczko A, Chowanski S, Marciniak P, Szymczak M, Spochacz M, Falabella P, Lelario F, Scrano L, Bufo S. Ultrastructural and developmental toxicity of potato and tomato leaf extracts to beet armyworm, *Spodoptera exigua* (Lepidoptera: Noctuidae). Microsc Res Tech. 2016;79:948–58. https://doi.org/10.1002/jemt.22726.
20. Büyükgüzel E, Büyükgüzel K, Snela M, Erdem M, Radtke K, Ziemnicki K, Adamski K. Effect of boric acid on antioxidant enzyme activity, lipid peroxidation, and ultrastructure of midgut and fat body of *Galleria mellonela*. Cell Biol Toxicol. 2013;29:117–29. https://doi.org/10.1007/s10565-013-9240-7.
21. Domingues CE, Abdalla FC, Balsamo PJ, Pereira BV, Hausen MA, Costa MJ, Silva-Zacarin M. Thiamethoxam and picoxystrobin reduce the survival and overload the hepatonephrocitic system of the Africanized honeybee. Chemosphere. 2017;186:994–1005. https://doi.org/10.1016/j.chemosphere.2017.07.133.
22. Ghotekar S, Pansambal S, Bilal M, Pingale S, Oza R. Environmentally friendly synthesis of Cr_2O_3 nanoparticles: characterization, applications and future perspective—a review. Case Stud Chem Environ Engine. 2021;3: 100089. https://doi.org/10.1016/j.cscee.2021.100089.
23. Sathish P, Dineshbabu N, Ravichandran K, Arun T, Karuppasamy P, Senthil Pandian M, Ramasamy P. Combustion synthesis, characterization and antibacterial properties of pristine ZnO and Ga doped ZnO nanoparticles. Ceram Int. 2021;47:27934–41. https://doi.org/10.1016/j.ceramint.2021.06.224.
24. Hassanein MS. Laboratory and outdoor cultures and breeding of locusts and grasshoppers. FAO Publ. 1965;5(31901):10.
25. Hunter-Jones P. Rearing and breeding locusts in the laboratory. London: Anti-locust Research Center; 1961.
26. Aldalbahi A, Alterary S, Almoghim RA, Awad MA, Aldosari NS, Alghannam SF, Alabdan AN, Alharbi S, Alateeq BA, Al Mohsel AA, Alkathiri MA, Alrashed AR. Greener synthesis of zinc oxide nanoparticles: characterization and multifaceted applications. Molecules. 2020;25:1–14.
27. Nakarungsee P, Srirattanapibul S, Issro C, Tang I, Thongmee S. High performance Cr doped ZnO by UV for NH3 gas sensor. Sens Actuators A Phys. 2020;314: 112230. https://doi.org/10.1016/j.sna.2020.112230.
28. Fathima AF, Mani RJ, Sakthipandi K. Enhanced antifungal activity of pure and iron doped ZnO nanoparticles prepared in the absence of reducing agents. J Inorg Organomet Polym Mater. 2020;30:2397–405. https://doi.org/10.1007/s10904-019-01400-z.
29. Shah AH, Ahamed MB, Neena D, Mohmed F, Iqbal A. Investigations of optical, structural and antibacterial properties of Al–Cr dual-doped ZnO nanostructures. J Alloy Compd. 2014;606:164–7. https://doi.org/10.1016/j.jallcom.2014.04.040.
30. Wang B, Iqbal J, Shan X, Huang G, Fu H, Yu R, Yu D. Effects of Cr-doping on the photoluminescence and ferromagnetism at room temperature in ZnO nanomaterials prepared by soft chemistry route. Mater Chem Phys. 2009;113:103–6. https://doi.org/10.1016/j.matchemphys.2008.07.031.
31. Chinnasamy M, Balasubramanian K. Enhanced UV photodetection behavior of Cr doped wurtzite ZnO crystalline nanorods. Opt Mater. 2020;110:110492. https://doi.org/10.1016/j.optmat.2020.110492.
32. Irshad K, Khan MT, Murtaza A. Synthesis and characterization of transition-metals-doped ZnO nanoparticles by sol–gel autocombustion method. Physica B Condes Matter. 2018;543:1–6. https://doi.org/10.1016/j.physb.2018.05.006.
33. Kondo M, Matsumoto J. Surface tension and wettability calculation using density gradient potential in a physically consistent particle method. Comput Methods Appl Mech Eng. 2021;385: 114072. https://doi.org/10.1016/j.cma.2021.114072.
34. Pandey PK, Chauhan V, Dixit P, Pandey PC. Correlation of enhanced photocurrent with structural and optical properties of Ag–ZnO nanocomposites synthesized by a facile chemical route. Physica B. 2021;612: 412937. https://doi.org/10.1016/j.physb.2021.412937.
35. Basith MN, Vijaya J, Kennedy LJ, Bououdina M, Jenefar S, Kaviyarasan V. Co-doped ZnO nanoparticles: structural, morphological, optical, magnetic and antibacterial studies. J Mater Sci Technol. 2014;30:1108–17.

36. López-López J, Tejeda-Ochoa A, López-Beltrán A, Herrera-Ramírez J, Méndez-Herrera P. Sunlight photocatalytic performance of ZnO nanoparticles synthesized by green chemistry using different botanical extracts and zinc acetate as a precursor. Molecules. 2022;27:6. https://doi.org/10.3390/molecules27010006.
37. Chand P, Gaur A, Kumar A. Effect of Cr and Fe doping on the structural and optical properties of ZnO nanostructures. Int J Chem Nucl Mater Metall Eng. 2014;8:1238–41. https://doi.org/10.5281/zenodo.1097046.
38. Kakati N, Jee SH, Kim SH, Oh JY, Yoon YS. Thickness dependency of sol–gel derived ZnO thin films on gas sensing behaviors. Thin Sol Films. 2010;519:494–8.
39. Xu L, Li X, Chen Y, Xu F. Structural and optical properties of ZnO thin films prepared by sol–gel method with different thickness. Appl Surf Sci. 2011;257:4031–7. https://doi.org/10.1016/j.apsusc.2010.11.170.
40. Bouderbala M, Hamzaoui S, Amrani B, Reshak AH, Adnane M, Sahraoui T, Zerdali M. Thickness dependence of structural, electrical and optical behaviour of undoped ZnO thin films. Phys B Condens Matter. 2008;403:3326–30. https://doi.org/10.1016/j.physb.2008.04.045.
41. Srinet G, Kumar R, Sajal V. Structural studies and band gap tuning of Cr doped ZnO nanoparticles. AIP Conf Proc. 2014;1591:1476. https://doi.org/10.1063/1.4873001.
42. Boulahlib S, Dib K, Ozacar M, Bessekhouad Y. Optical, dielectric, and transport properties of Ag-doped ZnO prepared by Aloe Vera assisted method. Opt Mater. 2021;113: 110889. https://doi.org/10.1016/j.optmat.2021.110889.
43. Tarwal NL, Shinde VV, Kamble AS, Jadhav PR, Patil DS, Patil VB, Patil PS. Photoluminescence and photoelectrochemical properties of nanocrystalline ZnO thin films synthesized by spray pyrolysis technique. Appl Surf Sci. 2011;257:10789–94. https://doi.org/10.1016/j.apsusc.2011.07.099.
44. Arrese EL, Soulages JL. Insect fat body: energy, metabolism and regulation. Annu Rev Entomol. 2010;55:207–25. https://doi.org/10.1146/annurev-ento-112408-085356.
45. Carvalho RB, Andrade FG, Levy SM, Maria Â, Falleiros F. Histology and ultrastructure of the fat body of *Anticarsia gemmatalis* (HÜBNER, 1818) (Lepidoptera: noctuidae). Braz Arch Biol Technol. 2013;56:303–10. https://doi.org/10.1590/S1516-89132013000200016.
46. Cunha FM, Wanderley-Teixeira V, Teixeira AA, Alves LC. Ultrastructure and histochemistry of the fat body of *Anthonomus grandis* (Coleoptera: Curculionidae). Invert Reprod Dev. 2016;60:126–30. https://doi.org/10.1080/07924259.2016.1162855.
47. Roma GC, Bueno OC, Camargo-Mathias MI. Morphophysiological analysis of insect fat body: a review. Micron. 2010;41:395–401. https://doi.org/10.1016/j.micron.2009.12.007.
48. Price GM. Protein and nucleic acid metabolism in insect fat body. Biol Rev. 1973;48:333–75. https://doi.org/10.1111/j.1469-185X.1973.tb01006.x.
49. Rosell RC, Wheeler DE. Storage function and ultrastructure of the adult fat body in workers of the ant *Camponotus festinates* (Bukley) (Hymenoptera: Formicidae). Int J Insect Morphol Embryol. 1995;24:413–26. https://doi.org/10.1016/0020-7322(95)00008-R.
50. Tadbowski JM, Jones JC. Changes in fat body and oocytes during starvation and vitellogenesis in mosquito, *Aedes aegypti* (L.). J Morphol. 1979;179:185–264. https://doi.org/10.1002/jmor.1051590203.
51. Thomsen E, Thomsen M. Production of specific protein secretion granules by fat body cells of the blowfly *Calliphora erythrocephala*. Cell Tissue Res. 1978;193:25–33. https://doi.org/10.1007/BF00221598.
52. Wigglesworth VB. The storage of protein, fat, glycogen and uric acid in the fat body and other tissues of mosquito larvae. J Exp Biol. 1942;19:56–77. https://doi.org/10.1242/jeb.19.1.56.
53. Locke M, Collin JV. The sequestration of protein by the fat body of an insect. Nature. 1966;210:552–3.
54. Meng X, Nouara A, Niannian W, Peng L, Zhichao N, Xin D, Shuang L, Chen K. Effects of Ag nanoparticles on growth and fat body proteins in silkworms (*Bombyx mori*). Biol Trace Elem Res. 2017;180:327–37. https://doi.org/10.1007/s12011-017-1001-7.
55. Adamski Z. Exposure to carbaryl leads to ultrastructural changes and alters activity of antioxidant enzymes in *Spodoptera exigua* (Lepidoptera: Noctuidae). Invert Biol. 2007;126:191–201.
56. Catae AF, Roat TC, Oliveira AR, Nocelli RC, Malaspina O. Cytotoxic effects of thiamethoxan in the midgut and malpighian tubules of africanized *Apis mellifera* (Hymenoptera: Apidae). Microsc Res Tech. 2014;7:274–81. https://doi.org/10.1002/jemt.22339.
57. Nasiruddin M, Mordue AJ. The effect of azadirachtin on the midgut histology of the locusts *Schistocerca gregaria* and *Locusta migratoria*. Tissue Cell. 1993;25:875–84. https://doi.org/10.1016/0040-8166(93)90036-K.
58. Remedio RN, Nunes PH, Anholeto LA, Oliveira PR, Sá IC, Camargo-Mathias MI. Morphological alterations in salivary glands of *Rhipicephalus sanguineus* ticks (Acari: Ixodidae) exposed to neem oil with known azadirachtin concentration. Micron. 2016;83:19–31. https://doi.org/10.1016/j.micron.2016.01.004.
59. Scudeler EL, Garcia AS, Padovani CR, Pinheiro PF, Santos DC. Cytotoxic effects of neem oil in the midgut of the predator *Ceraeochrysa claveri*. Micron. 2016;80:96–111. https://doi.org/10.1016/j.micron.2015.10.005.
60. Scudeler EL, Garcia AS, Padovani CR, Santos DC. Action of neem oil (*Azadirachta indica* A. Juss) on cocoon spinning in *Ceraeochrysa claveri* (Neuroptera: Chrysopidae). Ecotoxicol Environ Saf. 2013;97:176–82. https://doi.org/10.1016/j.ecoenv.2013.08.008.
61. Scudeler EL, Padovani CR, Santos DC. Effects of neem oil (*Azadirachta indica* A. Juss) on the replacement of the midgut epithelium in the lacewing *Ceraeochrys a claveri* during larval-pupal metamorphosis. Acta Histochem. 2014;116:771–80. https://doi.org/10.1016/j.acthis.2014.01.008.

Publisher's Note